Optical Systems Design for a Stratospheric Lidar System

I. Stuart McDermid[1], Apostolos Deslis[2], and Mary L. White[2]

Jet Propulsion Laboratory

California Institute of'technology

1. Table Mountain Facility

P. o. Box 367

Wrightwood

California 92397-0367

2,.4800 Oak Grove Drive

Pasadena

California 91109-8099

Paper to be submitted to APPLIED OPTICS

Note to Editor/Publisher

Address Correspondence to Dr. I. S. McDermid

Tel: (61 9) 249-4262 Fax: (619) 249-5392

E-mail: mcdermid@tmf.jpl.nasa.gov (Internet)

U. S. Mail:
JPI.-Tablc Mountain Facility
P.O.Box 367, Wrightwood, CA 92397-0367

UPS/Federal Express/Etc.
JPL-Table Mountain Facility
End of Table Mountain Road, Wrightwood, CA 92397-0367

Abstract

The optical systems for the transmitter and receiver of a high-power lidar for stratospheric measurements have been designed and analyzed, in part using Code V. 'I'he system requirements and design results arc presented and explained, An important and driving factor of this design was the requirement for a small image diameter in the plane of an optical chopper to allow the high intensity lidar returns from the lower atmosphere to be shielded from the detection system. The resulting system has been constructed and is now in operation at the Mauna Loa Observatory, Hawaii, making regular measurements of stratospheric ozone, temperature and aerosol profiles.

I. INTRODUCTION

The development of a differential absorption lidar (DIAL) for measurements of stratospheric ozone and for potential inclusion in the Network for the Detection of Stratospheric Change (NDSC)[1] began at JPL in 19S6. The original DIAL system at the JPL Table Mountain Facility (TMF, 34.4° N, 117.7° W) was developed specifically to have the characteristics suitable for long-term measurements as proposed for NDSC. Regular measurements of stratospheric ozone concentration profiles commenced in February 1988 and this system has been fully described previously [2,3]. The same system is also be used to make temperature and aerosol measurements using the return signals at the DIAL reference wavelength.

To evaluate the quality of the results from the TMF ozone lidar, it has participated in a number of intercomparisons 4-6 culminating in the first formal NDSC sponsored intercomparison, Stratospheric Ozone Intercomparison Campaign 1989 (STOIC) 7. These studies compared the results from a large number of ozone profiling instruments and showed that agreement at the So/O level could be achieved when the measurements were made at approximately the same time and at the same location.

Based on the successful demonstration and evaluation of the lidar system at TMF[4-7], a new project was initiated to develop an additional, similar system to participate in the Correlative Measurements Program for the Upper Atmosphere Research Satellite (UARS) and for deployment at the Mauna Loa Observatory, Hawaii, station of the NDSC (MLO, 19.5° N, 155.6° W). The entire optical system for the new lidar was redesigned, making usc of the computer aided design (CAD, Code V) capabilities at JPL. The new system builds on the lessons learned from the TMF lidar and also incorporates some recent developments in laser and electronics technologies. Overall, substantial improvements to the performance of the lidar, compared to the TMF system, have been achieved, This paper presents complete details of the optical design of this new lidar system.

The upper altitude for ozone profile measurements with the TMF lidar is limited by signal-induced-noise (SIN) which greatly reduces the signal-to-noise ratio (SNR) from what is predicted for this system. The SIN is caused by exposure of the photomultiplier detectors to the very intense lidar returns from the lower atmosphere. Electronic gating of the photomultipliers is found to reduce the level of SIN somewhat but the background signal level, especially for the 30S nm high intensity channel, is still affected by SIN. This is not unexpected since the photocathodes are still exposed to this high intensity pulse even though the amplification chain is interrupted. "l'he optimum solution is therefore to physically block the lidar returns below, say, 10 km using a chopper. However, in order to achieve the maximum blocking there needs to be a rapid transition of the chopper from the fully closed to fully open position. This means that the chopper blade must have a high velocity through the optical image and that the diameter of the image be as small as possible. There are severe practical limits to how fast the chopper blade can move. As described below, the chopper used in the new system has a velocity of 560 $m.s^{-1}$ at the chopping point. Thus, for example, to have a fully off to fully on transition equivalent to 2 km requires an image size of less than 1 mm diameter. To achieve this with large aperture (-1 m) telescopes is not trivial. The TMF telescope has a 0.9 m aperture with a f?? focal ratio and a low quality primary mirror (i.e., a light bucket). The combination of aberrations and image blur circle are on the order of 20 mm diameter and attempts to reduce this using auxiliary optics have largely failed because of the poor quality of the image. Control of the image quality and diameter were therefore important drivers in the design of the new receiver optics, However, also important were the cost of the telescope which was limited to $100K which means that the mirrors would not be of astronomical quality and the budget oft olerances and aberrations must be carefully accounted.

11. TRANSMITTER

By definition, differential absorption lidar requires the transmission of (at least) two wavelengths; one located in an absorption feature of the species of interest and one in a region of lower or no absorption by this species. The difference in magnitude of the absorption cross-section at the two wavelengths, the differential absorption cross-section, ultimately determines the sensitivity of the technique. In this implementation, the absorbed wavelength is 307.9 nm and the reference wavelength is 353.2 nm. These wavelengths are provide by a tuned xenon chloride (XeCl) excimer laser and the first Stokes Raman shift of the XeCl fundamental in hydrogen gas. Alternatively, the reference wavelength can be obtained from the xenon fluoride (XeF) fundamental at 351.1 nm.

A. Laser Systems

The laser system utilizes two LPX series lasers from Lambda Physik which were designed to match the required specifications for this lidar experiment. Each LPX laser comprises two separate excimer laser discharge units. The first unit, LPX-1 50, is set up in an oscillator-amplifier configuration which offers the capability of tunable, narrow-bandwidth, high-power laser operation. A diagram of this device is shown in figure 1. The oscillator can be tuned in wavelength by a motor controlled grating in conjunction with a prism beam expander. The output from this unit is then used to injection lock a power amplifier which is designated as the prc-amplifier in figure 1. The complete operation of these lasers, including the temporal synchronization, is controlled by a micro-computer, All signals between the laser and computer arc transmitted by a fiber-optic local area network (LAN), The energy output from each individual discharge unit is also monitored by the computer and the system can be programmed to maintain constant output power. A permanently mounted diode laser aids in the alignment of the laser cavities.

The LPX-250 contains two power amplifiers an this unit has similar micro-computer control and laser energy monitors. There are a number of possible configurations for the set-up of the complete four-laser system but only three are relevant to this experiment. Two of these options are shown in figure 2. In figure 2(a) the oscillator injection locks the pre-amplifier and the output is then single-passed through two amplifiers in series. In theory this arrangement should provide the highest laser output power. However, the same arrangements are possible with the laser system in the TMF lidar 3 and it has been found that losses between the two final amplifiers, caused for example by dirty windows, can severely reduce the final output power and the arrangement shown in figure 2(b) provides a more consistent output power level. In this arrangement the output from the pre-amplifier is split with the majority of the energy, >95%, being single-passed through the power amplifier. The remaining energy is then used to injection lock the other power amplifier. The output power from the injection locked amplifier is typically about 75°/0 of that from the single-passed amplifier. The configuration in figure 2(b) is the preferred arrangement when the system is operated with XeCl in all discharge volumes. In this situation the output from the injection locked amplifier is passed through a cell containing high purity hydrogen at approximately 500 psig in order to generate the reference wavelength 8-11 at 353.2 nm wavelength by stimulated Raman shifting. It is possible to operate the LPX-250 with different gas mixtures in each of the discharges, i.e., a two-color mode. For this application one discharge would act as a single-pass amplifier for XeCl as in figure 2(b), The second discharge would operate with XeF and an unstable resonator cavity, again similar to figure 2(b) but with no injection seeding. The two-color mode of operation provides more energy at the reference wavelength at the expense of some energy at 307.9 nm. For the stratospheric ozone D]AI.. experiment, normally only about 10°/0 of the energy is required at the reference wavelength compared to the probe wavelength. However, the Raman augmentation technique (see section IIIC) may require higher energy at the reference wavelength to obtain good signal-to-noise ratios in the

Raman reference channel. Since the reference wavelengths from Raman shifting the XeCl fundamental in H2 or from the XeF fundamental are quite close, the only elements of the optical detection system that need to be changed to switch between these wavelengths are the interference filters. A summary of the laser output specifications is given in Table I.

B. Laser beam-expan ders

To reduce the divergence of the output laser beams they are expanded by a factor of 5 before being transmitted into the atmosphere. This is important since it allows the field-of-view of the receiver telescope to be reduced which, in turn, reduces the size of the image in the plane of the chopper (see also section 1111]).

The laser beam expanders are afocal, recentered pupil, Dall-Kirkham telescopes, The primary mirror is a recentered section of a concave ellipsoid and the secondary mirror is a convex sphere. The collimated input beam strikes the convex sphere and diverges to fill the concave primary mirror which acts as the system aperture stop. The secondary mirror mount has a micrometer driven focus adjustment which can be used to compensate for divergence in the input laser beam or to converge the output beam towards a near field object/image point. The system is athermalized by means of an Invar metering rod that is attached to the base of the primary mirror and to a flexure mounted block that secures the focusing micrometer on the secondary mirror mount. This arrangement maintains a fixed spacing between the primary and secondary mirrors. The design of these beam expanders was ray-traced and tolerance using Code V and the optical parameters and specifications are given in Table II.

C. Beam stewing system

The expanded laser beams are steered into the atmosphere, and aligned to the receiver telescope, using 150 mm diameter gimbal-mounted flat mirrors. The gimbal mounts are

adjusted using servo controlled DC motor drives with integral 0.1 μm resolution position encoders. The design of the optical mounts is such that 0.1 μm (1 encoder unit) linear motion of the actuator translates to 1.0 prad angular position change, Each mount axis and associated linear actuator was carefully calibrated to establish precise backlash and drivetrain error compensation factors which were then programmed into the motion controller. Repeatable positioning accuracy to better than 5 μrad has been demonstrated with this system,

A schematic diagram of the computer controlled system and arrangement for aligning the laser beams to the telescope field-of-view is shown in Fig. 3. The alignment can be made manually, interactively or automatically. The general procedure is that a photomultiplier and gated photon counter are set up to observe, the atmospheric backscattered signal from any altitude range, e.g., between 45 and 50 km. The position of the laser beam is then swept through the field-of-view of the telescope, in orthogonal directions and plots of the signal level as a function of encoder readout (angular position) are obtained. By iterating these adjustments the laser beam can be accurately centered in the telescope field-of-view, at the selected altitude.

We have shown previously [3] that the alignment plots can be used to obtain measurement estimates of the telescope ficl(i-of-view and the divergence of the laser beams, Fig. 4 shows an actual example of the normalized signal count as a function of encoder angle, compared to a simple model based on overlapping circles. The overlap model allows the telescope field-of-view and the laser divergence to be changed in order to obtain the best agreement with the observed data. For this example, the telescope full field-of-view was set to 730 μrad and the laser divergence to 400 μrad in the model. It should be noted that the definition of the laser divergence for this model is that it is the angle that encompasses essentially all of the laser energy. These numbers arc in good agreement with expectations based on the system specifications.

III. RECEIVER

The receiver optical systems considered in the computer optimization include a telescope, field stop, field lens, relay lens, collimator and beamsplitters. The system was designed for high transmittance and for minimum image spot size in the chopper plane. The system was also required to maintain good performance over a large temperature range,

The optical system was modeled in Code V as three zoom positions with two focal planes, representing the image plane of the fore-optic and the chopper plane, and the third zoom position having an afocal lens module at the position of a detector. The system was modeled in three zoom positions so that fabrication and alignment tolerances could be determined based on the criterion of acceptable image quality at the three planes of interest.

A. Telescope

The receiver fore-optic is a 1-meter aperture Dall-Kirkham telescope with a focal ratio of f/8, which has good performance over the small field-of-view. As is shown in Fig. 5, the optical path is folded out of the side of the telescope to minimize the height since it was required to be housed in a container less than 2.7S m high. The obscuration of the primary aperture is less than 10°/0 and the mirror reflectivities are greater than 90°/0 for the UV wavelengths used. The elliptical primary mirror was fabricated from 47,5 mm (1 .875") thick slumped Pyrex and is mounted on a 9-point flotation mount. The structure is a Surrier Truss fabricated from 410 stainless steel **which** was selected for its low temperature expansion coefficient (CTE = 1.17 x 10-5 'C1). It was specified that, as built, the diameter of the 90% encircled energy at the focal plane, due to a point source, should be less than 0.5 mm over the temperature range from O to 30°C. The room temperature performance of the fore-optic was tested in a double-pass configuration with a knife edge while the performance at the extreme temperatures was predicted by analysis.

An adjustable iris diaphragm can be placed at the focus of the fore-optic for the purpose of limiting the field-of-view.

B. Relay **and chopper**

The field stop is followed by a field lens, which is used to reimage the pupil, and by a triplet, as shown in Fig. 6, which reduces the image formed by the telescope. This triplet operates at f/4, forming an image in the chopper plane of 0.083 mm diameter for a single point in the telescope field-of-view, Tolerances on the telescope and relay were determined based on the criterion that the image blur due to imperfect imagery should not increase the image size by more than 20°/0 compared to the ideal case. Fig. 7 shows the geometric spot diagrams for three points corresponding to the limits of the telescope field-of-view, ± 250 μrad, and on axis. The full field-of-view of the telescope is thus encompassed by a 2.28 mm circle at the chopper plane, or image plane of the relay triplet.

A rotating chopper is located at the image plane of the relay triplet, This chopper uses an 200 mm diameter, bowtie type blade rotating at 6000 rpm which provides openings corresponding to the 200 Hz experiment and laser repetition rate. At the chopping diameter the blade speed is 560 m s]. For the specified 2.28 mm image diameter from the relay triplet, the time for the chopper transition from fully closed to fully open is 40 μs, or 6 km in the lidar return. Since the laser does not fill the telescope field-of-view, these values represent upper limits and in practice, as is shown in figure 8, the lidar signal is chopped in approximately one third of theses times, i.e., 14 μs or 2.1 km.

After the chopper, the diverging light is collimated with only a singlet lens, Fig. 9, since image quality is no longer an important consideration. The entrance pupil of the telescope is imaged onto the detectors by the field lens. The size of the beam at the detector is 41 mm diameter for an on-axis point and 37 x 38 mJn for a point 250 pi-ad off-axis, with the difference being due to pupil aberration of the optical system. The geometric spot

diagrams shown in Fig. 10 for detector planes at various distances from the collimating lens and for the two wavelengths (308 and 353 nm) show that the detector active area (46 mm diameter) safely encompasses all of the received radiation.

The optimum detector location for each wavelength can be determined by tracing rim rays from field angles of ±250 prad, and finding the distance from the collimating lens at which these rays cross. However, physical limitations may ultimately determine where the detectors are placed. It is the usual practice of the optical designer to define the image of a pupil by determining the location where a paraxial chief ray crosses the optic axis but, when the large amount of pupil aberration and the lig,ht-bucket mode of operation are taken into account, it was decided that real marginal rays were the better choice as they would actually bound the size of the beam incident on the detector. The difference in the two methods gives a difference in position of about 75 mm.

C. Optical detection system

Stratospheric aerosols resulting from the volcanic eruption of Mt. Pinatubo have been observed in the lidar measurements at TMF since July 1991. The presence of these aerosols has a profound effect on measurements of stratospheric ozone profiles by the conventional DIAL method and reliable measurements in these regions are essentially precluded. A modification to the DIAL technique using the atmospheric nitrogen Raman signal has been suggested and demonstrated by the NASA-GSFC Lidar Group [12]. This method, similar to the Raman augmentation technique for temperature and density measurements [13,14], provides return signals form molecular scattering only and thus eliminates the problems caused by the differential aerosol backscattering. This technique is easily implemented by adding two extra channels to the lidar receiver which is shown in figure 11. Since it was necessary previously to attenuate the signal from altitudes below

about 30 km [3,7], the lower efficiency of the Raman scattering is largely compensated by eliminating the attenuation in these channels.

Figure 11 is a schematic diagram of the optical receiver system. After the relay and chopper which were described above, the received optical radiation is collimated by lens L2. The component wavelengths are then separated by a series of long-wave-pass beamsplitters S 1 -S3 which operate at 15° angle of incidence (not 45° as suggested by the schematic), These splitters have a specified reflectivity y of >98% at the selected wavelength and a specified transmission of >80% for the longer wavelengths. Operation at 15° angle of incidence, compared to 45°, increases the slope of the transition from reflective to transmissive. An example of the transmission curve for the 308 nm beamsplitter, measured in our laboratory using an IBM UV/Visible spectrophotometer, is shown in figure 12. Similarly shaped curves are obtained for the other wavelength beamsplitters. Thus, the beamsplitter S 1 reflects 308 nm at >98% efficiency and transmits 332, 353 ant{ 385 nm with >90% efficiency; S2 reflects 332 mn and transmits 353 and 385 nm, and so on,

A second beamsplitter, S4, operates in the 308 nm and 353 nm channels. These splitters are used to extend the dynamic range of the experiment and are quartz flats coated on both sides with a broadband uv-anti-reflection coating which results in an effective reflectivity on the order of 1% at 308 nm or 353 nm. Thus, the optical radiation is divided roughly in the ratio 100:1 providing two extra decades of useful signal. The lower intensity signals, inducting the Raman channels at 332 nm and 385 nm, are used to retrieve profiles only below approximately 35 km altitude. The higher intensity signals allow ozone measurements up to 50-60 km and temperature measurements to >75 km altitude.

An interference filter is placed in front of each detector to further increase the wavelength selectivity, reducing background] signal levels and eliminating cross-talk between the channels. These are 50 mm diameter, two-cavity type filters. An example of the transmission curve for the 353 nm interference filter, obtained in the same manner as the

beamsplitter curve in figure 12, is shown in figure 13. The peak transmission of this filter is 41 % and it has a full-width-half-maximum of 2 mn. The filters are also optically blocked to 650 nm where the response of the hi-alkali photocathodes in the detectors falls off rapidly.

The detectors are all fast, linear-focused photomultipliers, with hi-alkali photocathodes which arc optimal for the near uv wavelength region. The tubes are specially selected to have high gain at low bias voltage since this has been found to greatly reduce the effect and occurrence of signal-induced-noise. This tube type is also optimized for photon counting, which is the method used for signal measurement, and they have fast rise times on the order of 2 ns for single photon pulses. This is a necessary specification since the counting system electronics can operat c at up to 300 MHz which in turn requires single pulses to be <4 ns.

IV. SUMMARY

The lidar system described above has been installed into a mobile facility comprising two custom built, 40' long trailers. The laser transmitter and optical receiver systems are located in one trailer and the data acquisition and analysis systems, together with the laser heat exchanger and a general work area, comprise the second trailer. This arrangement helps to isolate the optical components from the vibrations caused by the heat exchanger and by personnel moving about, The design of the trailers allows them to be moved intact by road or ship, and the undercarriage can easily be removed for transportation by airplane or container-ship. The system underwent successful testing and intercomparison with the existing lidar at the JPL-Table Mountain Facility and was moved to Mauna Loa in July 1993 where it is now in routine operation. Stratospheric measurements from this system will be presented elsewhere.

Acknowledgments

The work described in this paper was carried out at the Jet Propulsion Laboratory, California Institute of Technology, under a contract with the National Aeronautics and Space Administration, We are grateful to Tom McGee for interesting discussions regarding the Raman augmentation to the DIAL technique.

References

1. M, J. Kurylo and S. Solomon, "Network for the Detection of Stratospheric Change. A Status and Implementation Report," issued by NASA Upper Atmosphere Research Program and NOAA Climate and Global Change Program (Jan. 1990).

2. I. S. McDermid, S. M. Godin and L. O. Lindquist, "Ground-based laser DIAL system for long-term measurements of stratospheric ozone," Appl. Opt. 29, 3603-3612 (1990),

3. 1. S. McDermid, D. A, Haner, M. M, Kleiman, T. D. Walsh and M. L, White, "Differential Absorption Lidar Systems for Tropospheric and Stratospheric Ozone Measurements," Opt. Eng. 30, 22-30(1991).

4. J. S. McDermid, S. M. Godin, P. 1-1. Wang and M. P. McCormick, "Comparison of stratospheric ozone profiles and their seasonal variations as measured by lidar and SAGE II during 1988," J. Geophys. Res. 95, S605-5612 (1990),

5. I. S. McDermid, S. M, Godin, L. O. Lindquist, T. D. Walsh, J, Burris, J. Butler, R. Ferrare, D. Whiteman and T. J. McGee, "Measurement intercomparison of the JPL and GSFC stratospheric ozone lidar systems," Appl. Opt, 29, 4671-4676 (1990).

6. I. S. McDermid, S. M. Godin, R, A. Barnes, C, L, Parsons, A. Torres, M. P. McCormick, W. P. Chu, P. Wang, J. Butler, P. Newman, J. Burris, R. Ferrare,

D. Whiteman and T. J. McGee, "Comparison of ozone profiles from ground-based lidar, ECC balloon sonde, ROCOZ-A rocket sonde, and SAGE II satellite measurements)" J, Geophys. Res. 9S, 10037-10042 (1990).

7. 1. S. McDermid, S. M, Godin and T. D. Walsh, "Results from the JPL stratospheric ozone lidar during STOIC 1989," submitted to J. Geophys. Res..

8. V. Yu. Baranov, V. M. Borisov, A. Yu. Vinokhodov. Yu. B. Kiryukhin and Yu. Yu. Stepanov, "Stimulated Raman scattering of radiation from an electric-discharge pulse-periodic XeCl laser in compressed H_2," Sov. J. Quantum Electron. **15,** 727-729 (1985).

9, V. Yu. Baranov, V. M, Borisov, A, Yu. Vinokhodov, D. V. Vlasov, Yu. B. Kiryukhin, D, N. Molchanov, V, P. Novikov, M. I. Persiantsev and J. V. Fedorov, "Conversion of λ=308 nm radiation at pulse repetition frequencies up to 600 Hz by stimulated Raman scattering in compressed hydrogen," Sov. J. Quantum Electron. **18,** 1272-1277 (1988).

10, Q. Lou, "Research on the characteristics of 1-12 Raman conversion pumping by a 1-J XeCl excimer laser," J, Appl. Phys. 66, 2265-2273 (1989).

11. D. A. Haner and 1. S. McDermid, "Raman shifting of Nd:YAG fourth harmonic (266 nm) in 1-12, HD and D_2," IEEE J, Quantum Electron. **QE-26**, 1292-1277 (1990).

12. T. J. McGee, M, R, Gross, R. A. Ferrare, W. S. l-leaps, and U, N. Singh, "Raman lidar measurements of stratospheric ozone in the presence of volcanic aerosols," Geophys. Res. Lett. 20,955-958 (1 993).

13. W. P. Moskowitz, G. Davidson, D. Sipler, C. R. Philbrick and P. Dao, "Raman augmentation for Rayleigh lidar," 14th ILRC, *Conference Abstracts, 284-286 (1988).*

14. P. D. Dao, w , Klemetti, D. Sipler, W. P. Moskowitz and G. Davidson, "Density measurements with combined Raman-Rayleigh lidar," Proc. SPIE, **1062,** 138-143 (1989).

Repetition Rate	200 Hz
Bandwidth	<3 pm
Divergence	<200 µrad
Beam 1- XeCl	307.9 **nm**
Pulse Energy	**300** mJ
Power	**60** W
Beam 2 - XeCl	307.9 nm
Pulse Energy	200 mJ
Power	40 W
Beam 2- XeF	351,1 **nm**
Pulse Energy	125 mJ
Power	2, W

Table 1. Laser specifications

Vertex radius of primary mirror	60.00 inches (concave)
Conic constant	-0.80 (plus higher order terms)
Secondary mirror radius of curvature	12.00 inches (convex)
Vertex separation	24.00 inches
Separation between input and output beam axes	4.01 inches
Output aperture diameter	6.00 inches (150 mm)
Input aperture diameter	1.18 inches (30 mm)
System magnification	5 x
Surface quality Primary mirror Secondary mirror	 60-40 S/D 10-5 S/D
Optical coatings, Reflectivity	R $\geq$ 97% at 308, 325, and 353 nm R $\geq$ 25% at 633 nm
System wavefront accuracy (at 633 nm)	Peak to valley <0.20 waves optical path difference R.M. S. wavefront accuracy 0.033 waves
Wavefront geometric divergence	12 microradians full angle

Table II. Beam expander optical parameters and specifications

	RADIUS OF CURVATURE			APERTURE DIAMETER		
ELEMENT	FRONT	BACK	THICKNESS	FRONT	BACK	GLASS
PRIMARY	See Below		-81.0000	40.00		REFL.
SECONDARY	-131.5778 CX		70.0000	13.36		REFL.
FOLD	Tilt 45° about axis		-34.9999	6.87		REFL.
PARAXIAL FOCUS			-0.0004			
			-0.1500			
FIELD	0.2087 CC	0.2417 CX	-0.2428	0.28	0.28	SILICA
	1 .		-1.7573			
RELAY 1	-1.3300 Cx	I .7400 Cx	-0.4215	0.20	0.19	SILICA
			-0.1526			
RELAY 2	0.7870 CC	0.9777 Cx	-0.4500	0.18	0.20	SILICA
			-0.1357			
RELAY 3	-0.6445 CX	1.5320 CX	-0.1678	0.21	0.21	SILICA
			-0.7500			
PARAXIAL FOCUS			.-0.0050			
			-6.1004			
COLLIMATOR	-15.9930 Cx	3.8000 CX	-0.5000	1.58	1.63	SILICA
			-23.4433	1		

Note: Dimensions in inches

PRIMARY MIRROR SURFACE $$z = \frac{(-0.0041\,1766)Y^2}{1+\left[1-(1-0.6067467)(-0.0041\,1766)^2 Y^2\right]^{1/2}}$$

Table III. Receiver optics specifications.

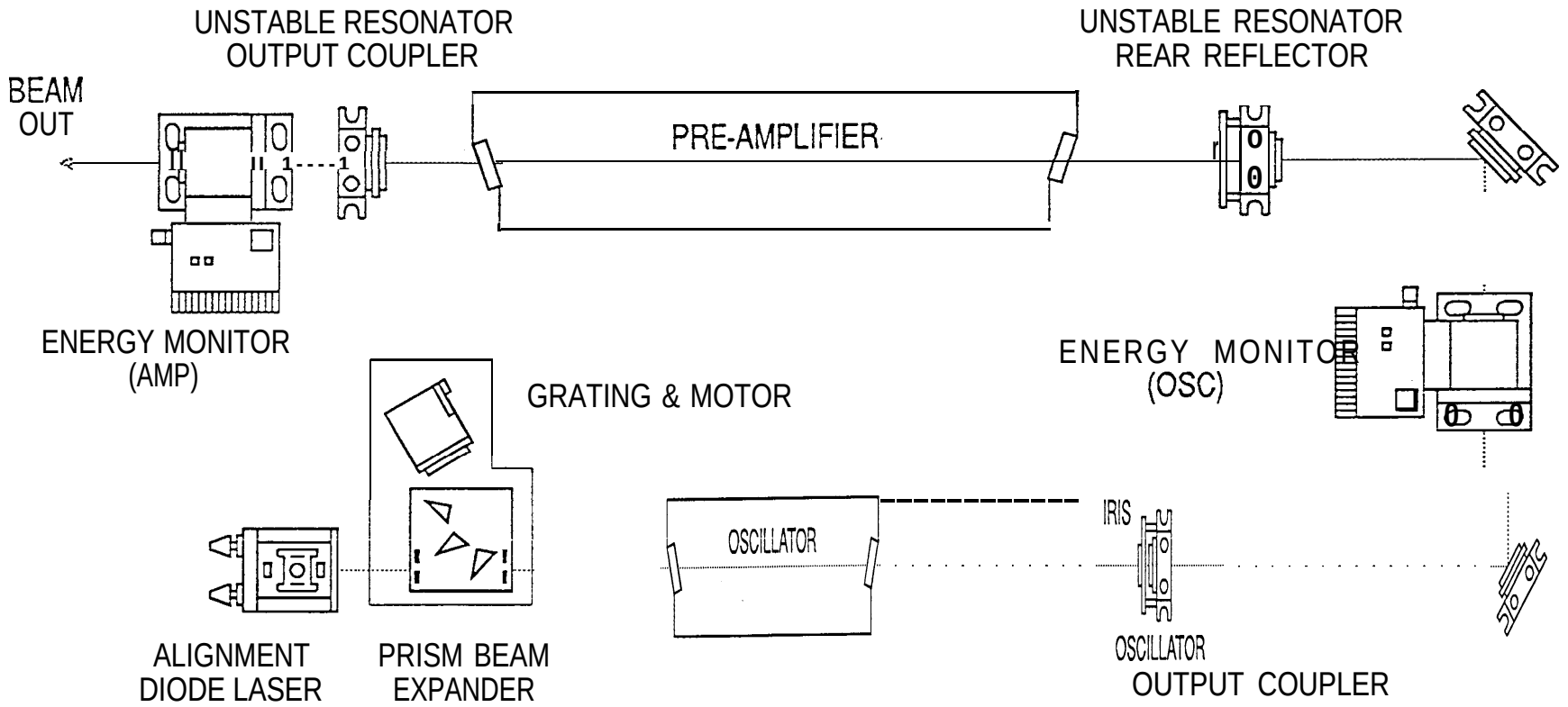

Figure 1. Diagram of the LPX-150 (Lambda Physik) tunable xenon chloride oscillator-amplifier laser system.

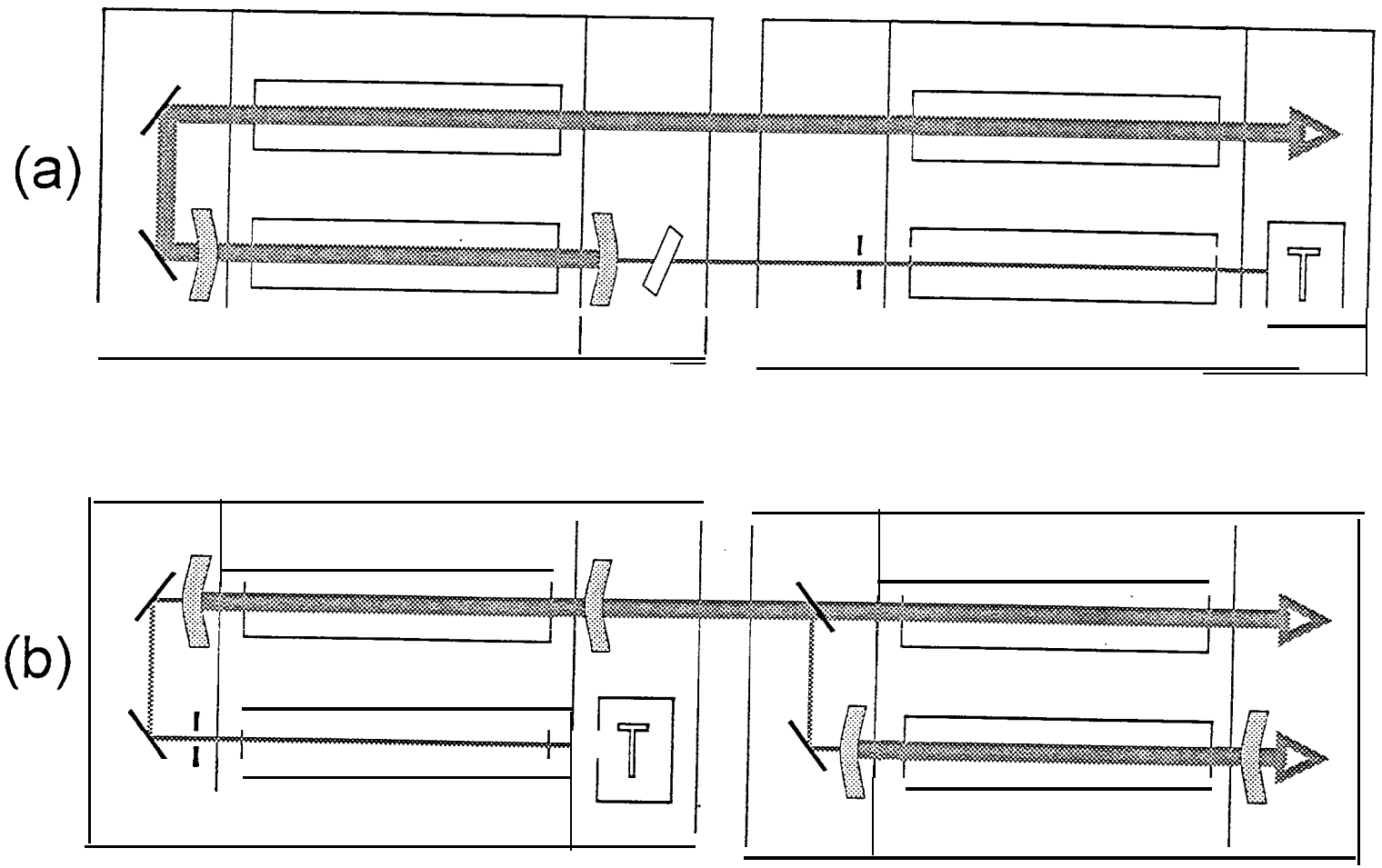

Figure 2. Two possible arrangements of the complete 4-laser system.

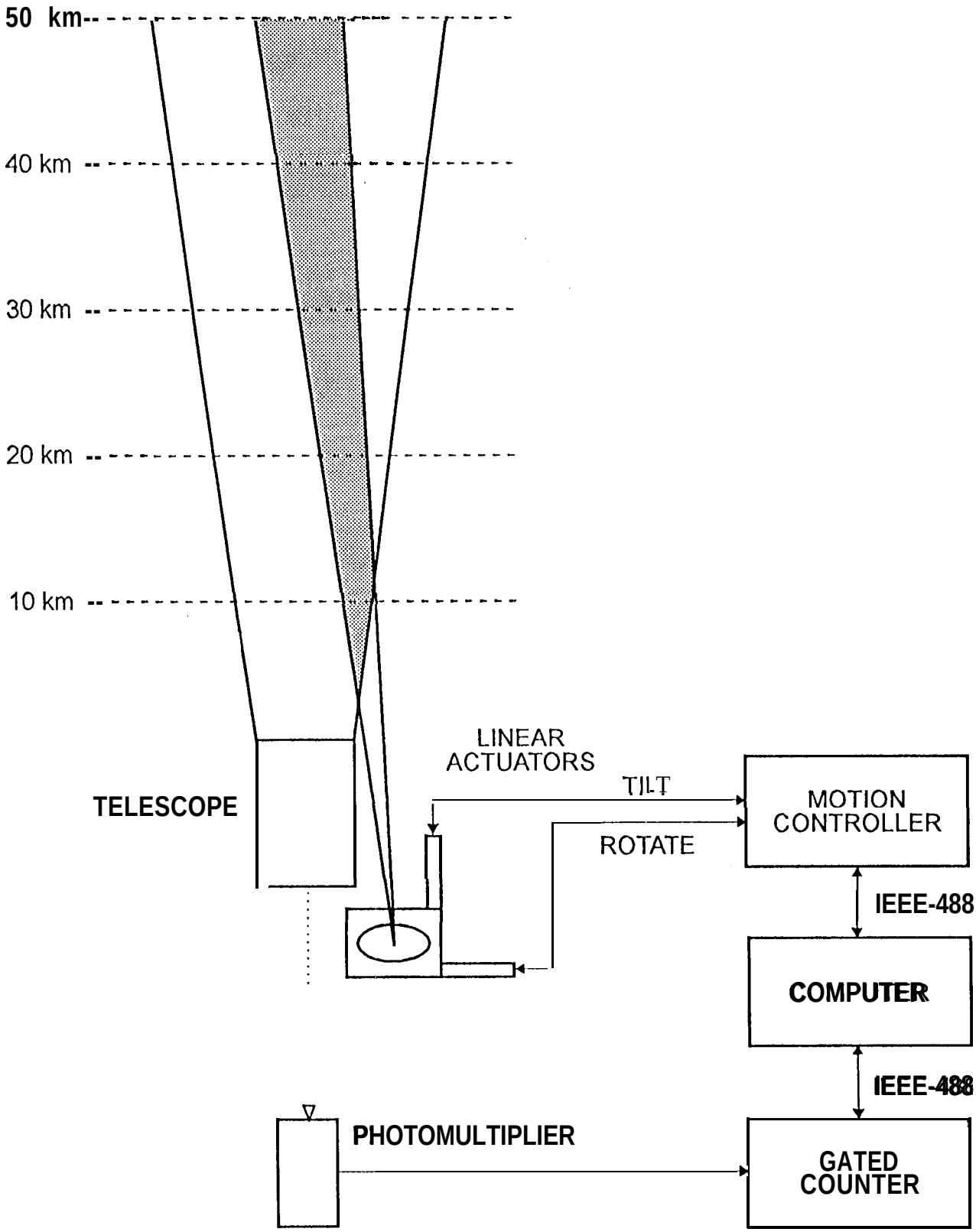

Figure 3. Schematic of the laser-telescope alignment and control sytsems.

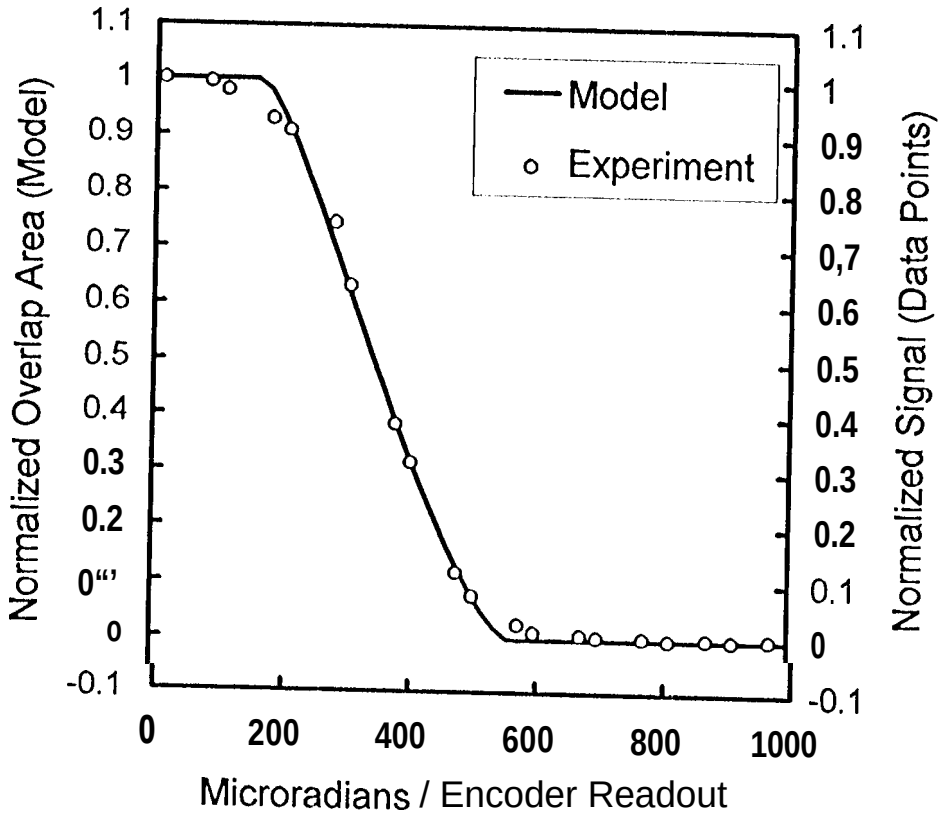

Figure 4. Laser-telescope alignment plot. Comparison of actual alignment data points with overlapping circles model with telescope FOV = 730 μrad and laser divergence = 200 prad.

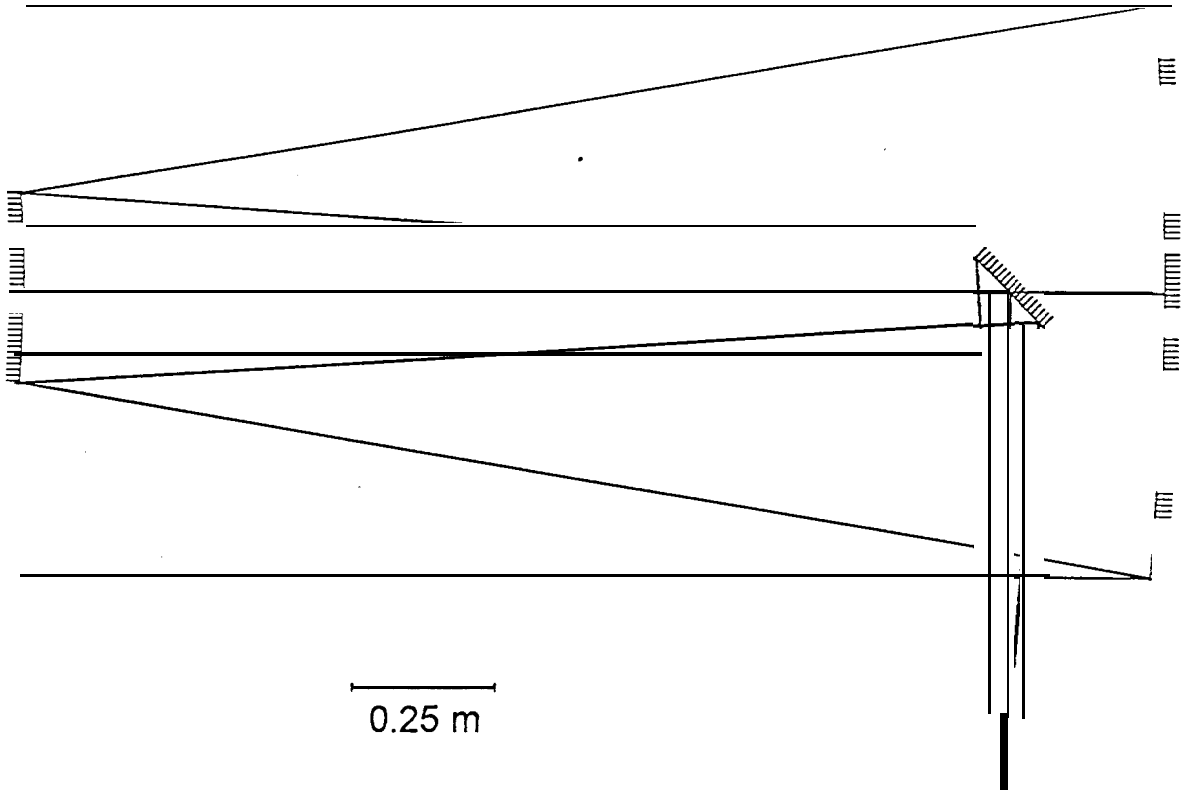

Figure 5. Scale diagram of the Dali-Kirkham telescope with folded optical path.

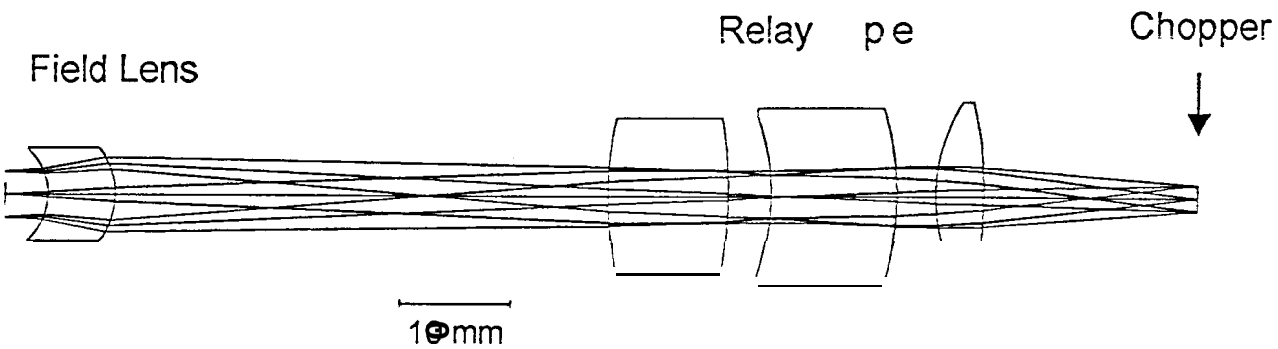

Figure 6. Scale of field lens and triplet.

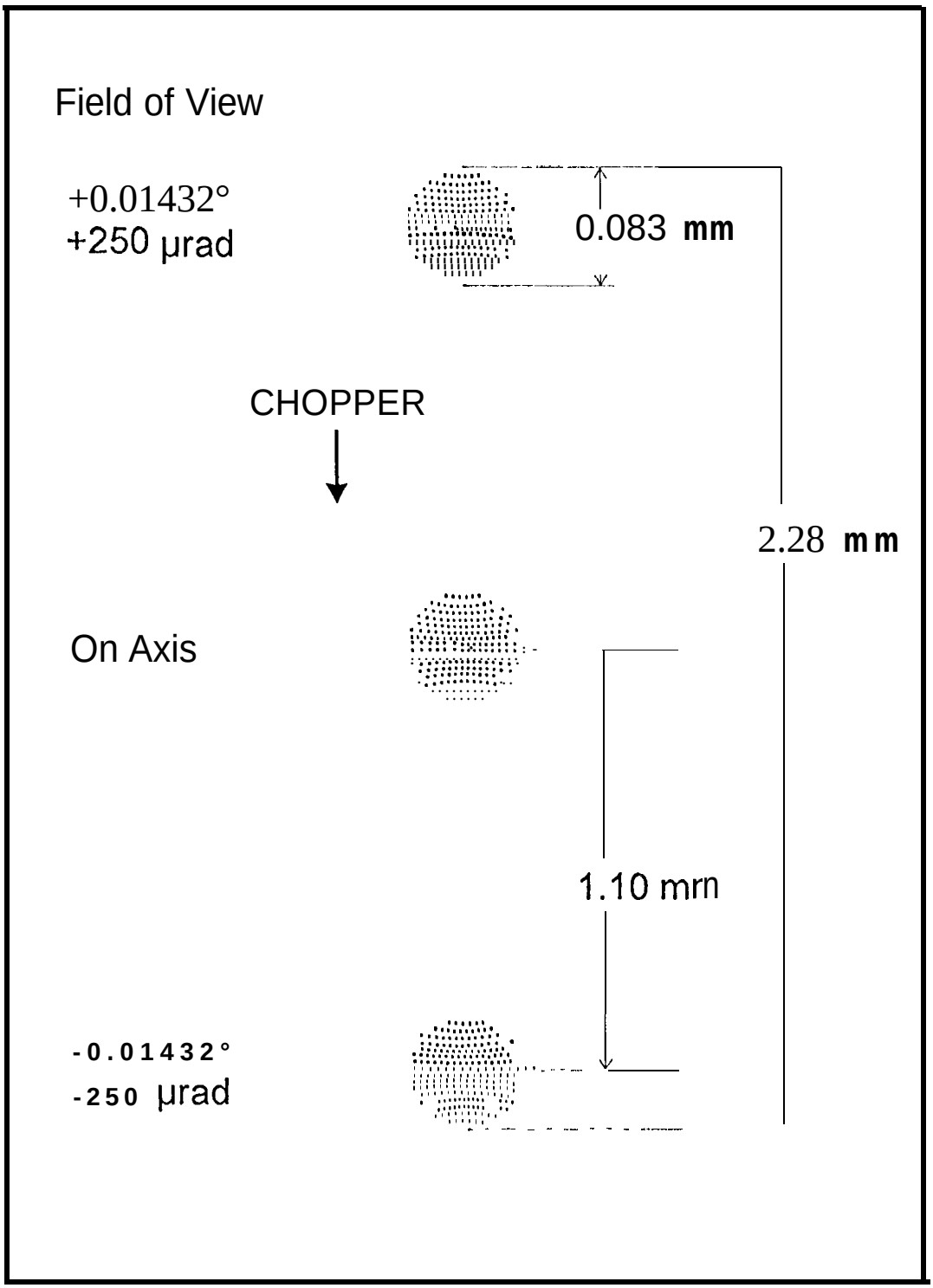

Figure 7. Geometric spot diagrams of the image in the chopper plane.

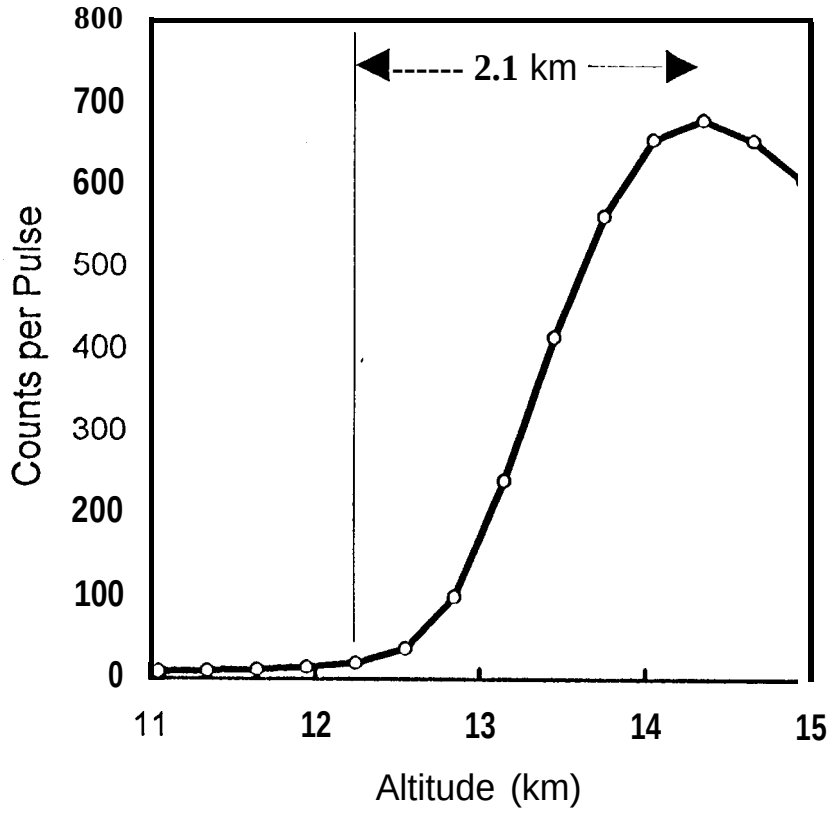

Figure 8. Expanded view of the segment of the lidar return signal showing the chopper opening transition. Fully closed to fully open is on the order of 2.1 km or 14 μs.

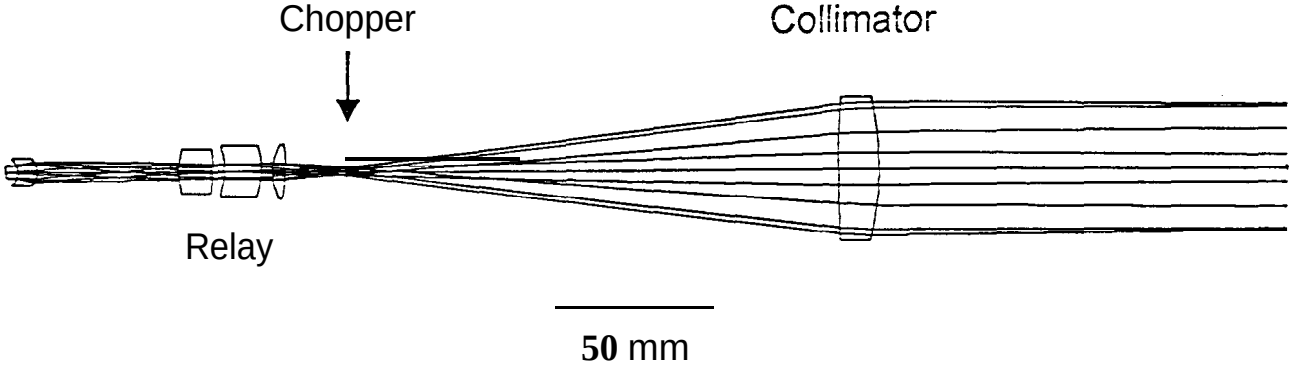

Figure 9. Scale diagram of the telescope aft-optics.

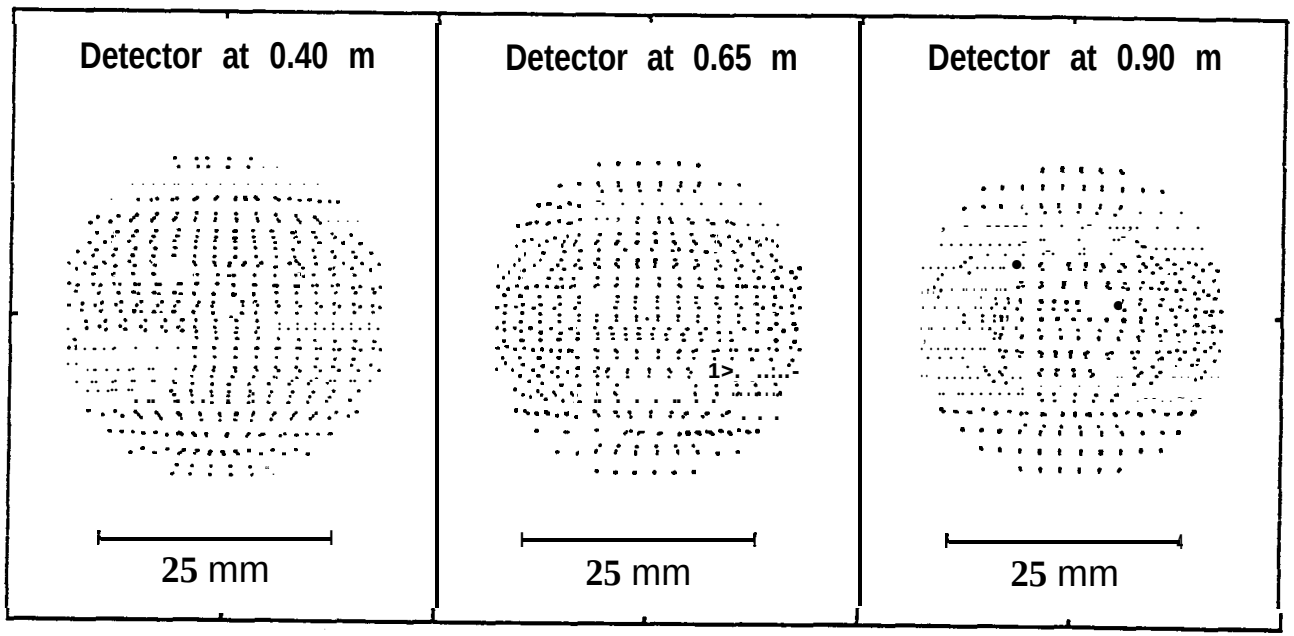

Figure 10. Geometric spot diagrams for detector planes at various distances from the collimator lens.

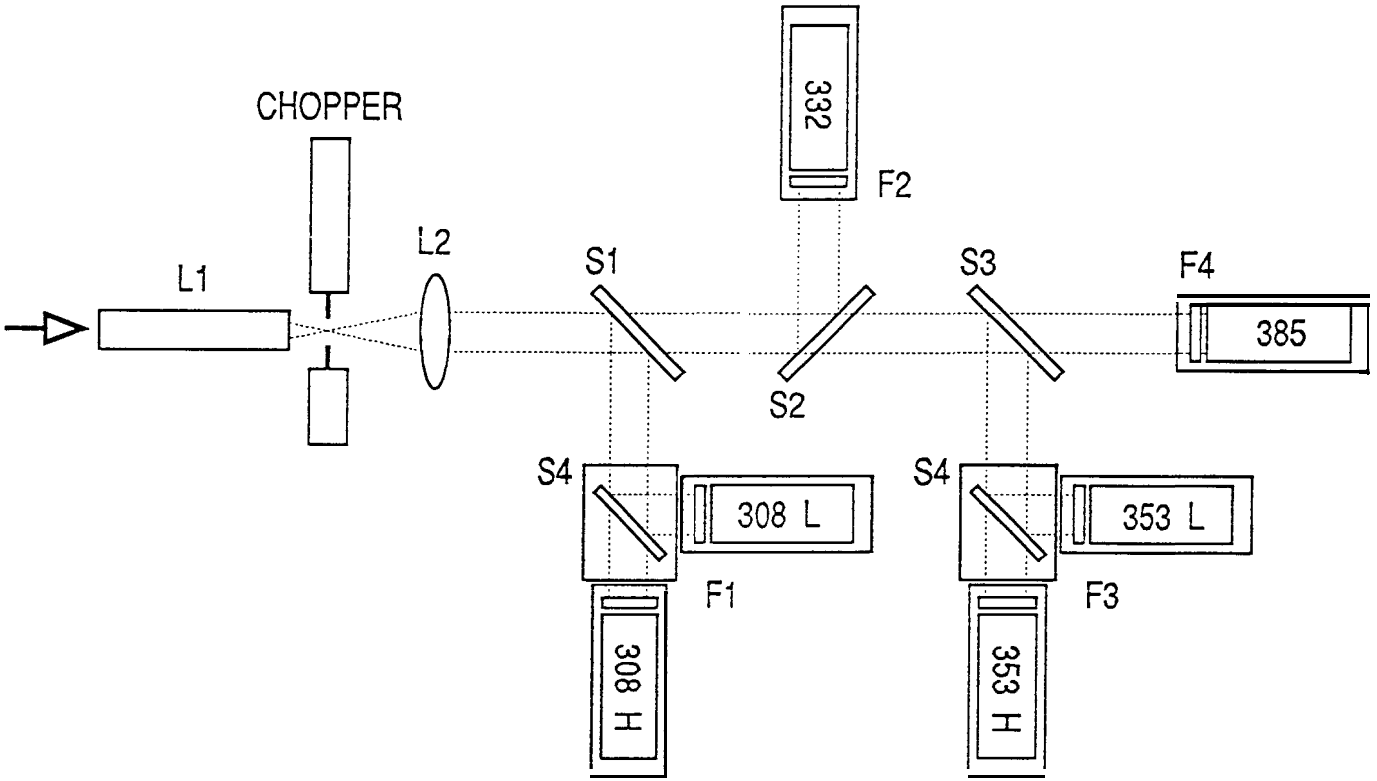

Figure 11. Schematic diagram of the optical detector system.

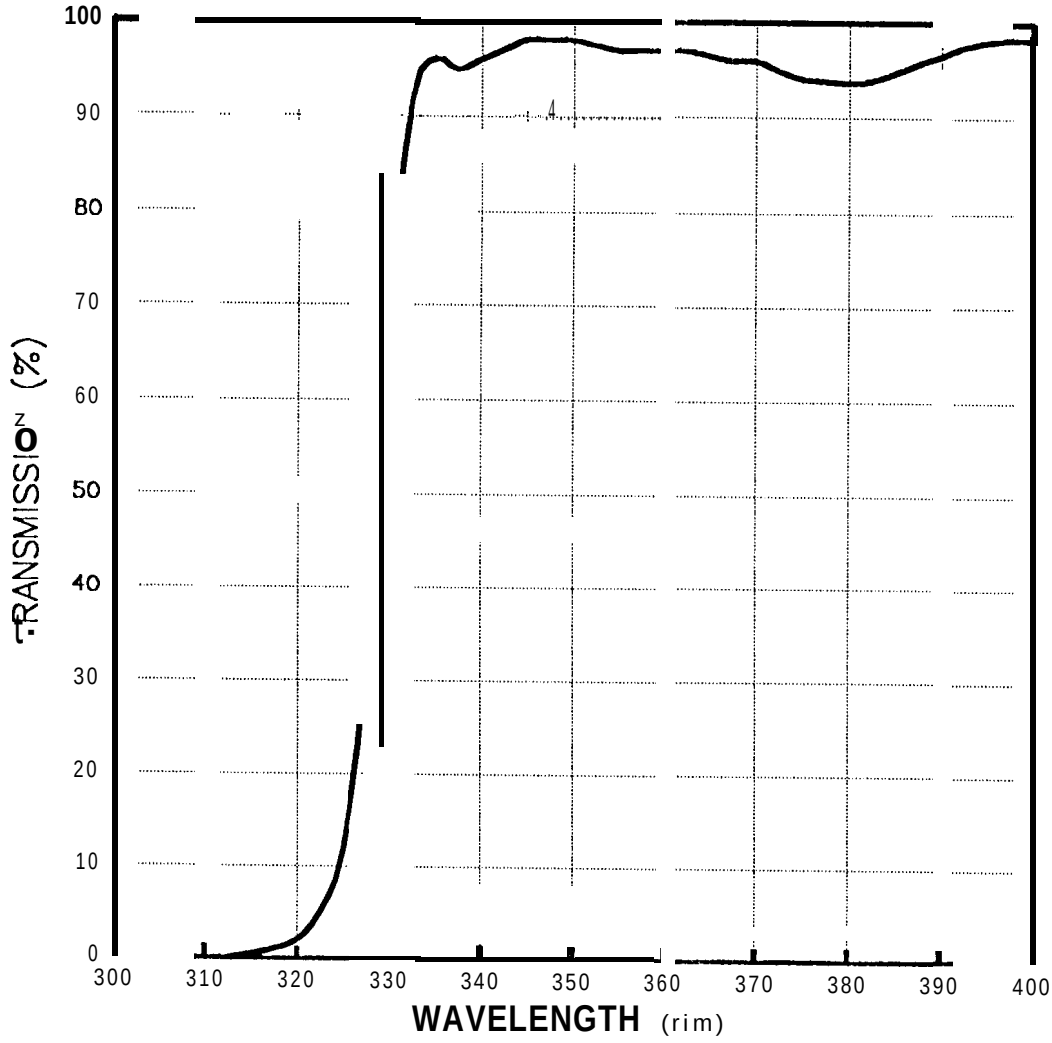

Figure 12. Transmission curve for the 30S nm long-wavelength-pass beamsplitter at 15° angle of incidence. The transmissions at 332, 353 and 385 nm are 85%, 97% and 94% respectively. Zero transmission is assumed to correlate with >98% reflection.

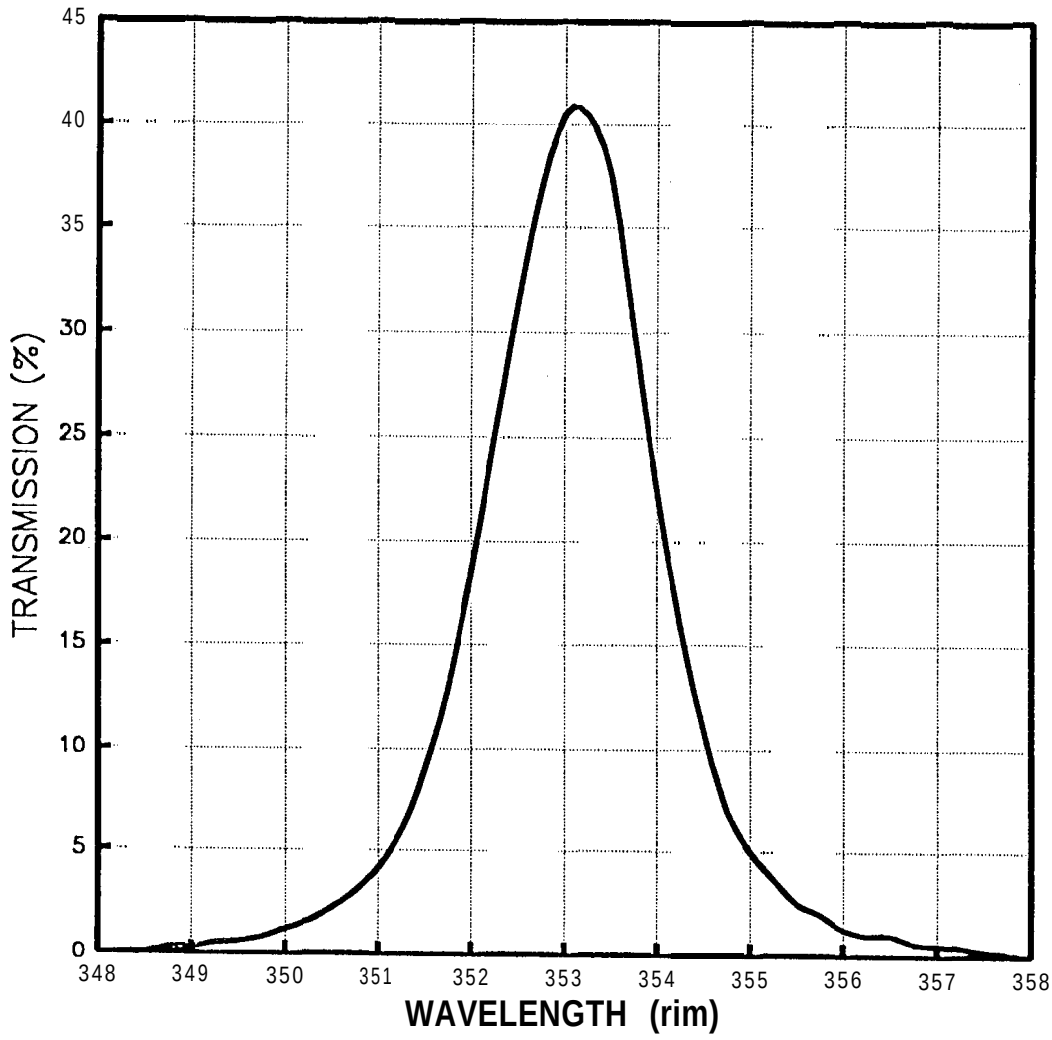

Figure 13. Transmission curve for the 353 nm interference filter. The peak transmission is41 % and the FWHM is 2 nm,